Reactive transport modelling to investigate multi-scale waste rock weathering processes

Nicolas Seigneur, B. Vriens, R.D. Beckie, K.U. Mayer

Reactive transport modelling to investigate multi-scale waste rock weathering processes

N. Seigneur[1,2], B. Vriens[3,2], R.D. Beckie[2], K.U. Mayer[2]

Abstract

Prediction of drainage quantity and quality is critical to reduce the environmental risks associated with weathering mine waste rock. Reactive transport models can be effective tools to understand and disentangle the processes underlying waste-rock weathering and drainage, but their validity and applicability can be impaired by poor parametrization and the non-uniqueness conundrum. Here, a process-based multicomponent reactive transport model is presented to interpret and quantify the processes affecting drainage quantity and quality from 15 waste- rock experiments from the Antamina mine, Peru. The deployed uniform flow formulation and consistent set of geochemical rate equations could be calibrated almost exclusively with measured bulk waste-rock properties in experiments ranging from 2kg to 6500 tons in size. The quantitative agreement between simulated dynamics and the observed drainage records, for systems with a variety of rock lithologies and over a wide range of pH, supports the proposed selection of processes. The controls of important physicochemical processes and feedbacks such as secondary mineral precipitation, surface passivation, oxygen limitations, were confirmed through sensitivity analyses. Our work shows that reactive transport models with a consistent formulation and evidence-based parametrization can be used to explain waste-rock drainage dynamics across laboratory to field scales.

Keywords:
Reactive Transport Modelling, acid rock drainage, water quality, coupled processes

1. Introduction

Mining operations around the world produce millions of tons of waste materials every year, including waste rock that is stored on-site in tall piles

Preprint submitted to Journal of Contaminant Hydrology *November 22, 2020*

Email addresses: nicolas.seigneur@mines-paristech.fr, nseigneur@eoas.ubc.ca (N. Seigneur), umayer@eos.ubc.ca (K.U. Mayer)

[1]MINES ParisTech, PSL University, Centre de géosciences, 35 rue St Honoré, 77330, Fontainebleau, France.

[2]Earth, Ocean and Atmospheric Sciences. University of British Columbia, Vancouver, Canada.

[3]Queen's Universitiy, Geological Sciences and Engineering, Kingston, Canada.

(Hudson-Edwards and Dold, 2015). Waste-rock piles require effective management to reduce environmental risks associated with the oxidation of minerals that can mobilize contaminants and lead to deterioration of downstream water quality, e.g., acid rock drainage (Akcil and Koldas, 2006; Lindsay et al., 2009; Amos et al., 2015). A quantitative understanding of the processes controlling waste-rock weathering and drainage rates is required to develop predictive models for strategic waste management planning. Similar to the so-called "5P" rule of economics, it can be said that *Proper Prediction Prevents Poor Performance*, for which reactive transport models constitute an attractive tool to disentangle the strongly coupled hydrogeochemical processes. Hence, a growing number of reactive transport modelling studies is dedicated to waste-rock piles (Linklater et al., 2005; Molson et al., 2012; Demers et al., 2013; Shokri et al., 2016; Lahmira et al., 2017; Pabst et al., 2017; Wilson et al., 2018). Additionally, reactive transport simulations offer the possibility to examine future reclamation scenarios, *e.g.* , the effectiveness of cover systems or co-disposal techniques(Haug and Pauls, 2002; Aubertin et al., 2009; Martin et al., 2017; Raymond et al., 2020b).

Various coupled physicochemical processes control the overall drainage dynamics of an exposed waste-rock pile (Amos et al., 2015). Principal geochemical reactions include primary sulfide, carbonate and silicate mineral dissolution and secondary mineral precipitation. Geochemical reaction rates are controlled by mineral abundance and particle size, i.e., reactive surface area (Erguler and Erguler, 2015), often aggregated to describe waste-rock reactivity (Lawrence and Wang, 1996; Blowes et al., 2003; Price, 2009; Elghali et al., 2019), and local geochemical conditions such as pH, oxygen concentration and temperature. Relevant physical transport processes include gas, heat and water transport through the unsaturated waste rock. Water infiltration is typically non-uniform in waste rock-piles that have a wide range of particle sizes; orders-of-magnitude discrepancies may exist between the transport times of drainage fronts and thus dissolved solutes. In addition, mineral dissolution and precipitation can impact reactive surface area and porosity and thereby associated physical transport parameters (Seigneur et al., 2019). Gas reactions, O_2 consumption and CO_2 production, induce concentration gradients that trigger diffusive gas transport, respectively: oxygen ingress has been shown to limit weathering rates in large systems with reactive materials (Vriens et al., 2019c). Furthermore, heat production from sulfide oxidation in large waste-rock piles can result in temperatures as high as 70C (Lefebvre et al., 2001) and induce thermal gas convection and im-

pact geochemical equilibria and reaction rates. All of the above processes are subject to vary with significant heterogeneity, from small-scale mineral impurities and textural variability to macroscale material heterogeneity, e.g., as a result of rock blending and structural features such as traffic surfaces (Atherton, 2017; Wilson et al., 2018; Raymond et al., 2020a). The predictive success of a mechanistic model relies on identifying and taking into account the relevant processes and heterogeneities.

It is unpractical and unrealistic to quantify all these processes, feedbacks, and heterogeneities existing in waste-rock piles. Reactive transport models are often constructed *as simple as possible, as complicated as necessary*, and incorporate only a select number of processes known or assumed to be relevant in the studied systems. This selection will change with the goal of the model (fit-for-purpose) and availability of field data to parameterize the considered processes, which complicates the deployment and cross-validation of reactive transport models between sites. Only in few cases is the exclusion of certain processes justified by actual field data, *e.g.* in-situ temperature measurements to estimate thermal convection Lefebvre et al. (2001). The number of model parameters increases with the number of considered processes, and over-parametrization for the sake of fitting is a valid concern when field data is limited and physical parameters are challenging to quantify, such as gas permeability, preferential flow in piles with boulder-sized waste rock. As a result, non-uniqueness, the multiple combinations of parametrized processes can be used to reproduce data Carrera and Neuman (1986); Bethke (2007), is of particular concern when interpreting reactive transport simulations of waste-rock systems. Finally, waste rock models are often parameterized with physicochemical properties from small-scale static and kinetic laboratory tests, but the values of model parameters determined at small scales often differ from those needed in models at larger spatiotemporal scales, i.e. hundreds of meters tall piles. Certain processes irrelevant to weathering rates in laboratory tests will gain significance at increasing scale (thermal gradients and gas-transport limitations, preferential flow phenomena). Scaling factors have been proposed to facilitate the extrapolation of laboratory parameters onto practice-relevant dimensions (Strömberg and Banwart, 1999; Malmström et al., 2000; Plante et al., 2014), but these are typically semi-empirical correction factors based on limited mechanistic evidence. Process-based reactive transport simulations constitute an alternative tool for waste-rock drainage prediction, provided that the critical processes and feedbacks are identified, and reliable data are available to characterize

these.

To this end, we developed a process-based reactive transport framework and use data from a long-term multiscale research program at the Antamina mine in Peru to investigate physicochemical processes in the weathering of waste rock. At Antamina, multiple types of waste rock have been extensively characterized (hydraulically, mineralogically and physically) and weathered at different spatiotemporal scales, providing a unique opportunity to quantify the relevance of individual weathering processes. We focus on processes that could be well-constrained experimentally (i.e. grain size, porosity, hydraulic parameters and mineralogy) and deploy a consistent model formulation across all experiments and waste-rock types. The adopted consistent model formulation is built on a one-dimensional uniform flow description for all investigated experiments, offering the opportunity for evidence-based parametrization. The limitations and scale dependence of the adopted model framework for larger-scale heterogeneous systems is the focus of an associated article (Vriens et al., 2020). This work uses the same model framework to examine individual processes underlying drainage dynamics across these experimental scales.

This work is structured as follows: section 2 describes the reactive transport formulation, parametrization and calibration; section 3 presents the observed drainage dynamics and simulation results and the overall implications of this work are discussed in section 4.

2. Materials and methods

2.1. Overview of the experimental program

Since 2005, an experimental program has been conducted at the Antamina mine (9° 32' 14.6" S, 77° 02'51.8"W), a large polymetallic (Cu, Zn, Mo) open-pit mine located at $\sim$ 4400 m altitude in the Peruvian Andes. Love et al. (2004) describe the geological setting of Antamina, one of the largest skarn deposits in the world, hosted by Cretaceous sedimentary rocks.Harrison et al. (2012) and Beckie et al. (2011) describe Antamina's waste-rock research program. This paper focuses on 15 experiments, grouped into four levels of increasing scale and complexity:

- Humidity test cells: 5 tests each consisting of 2 kg crushed waste rock (2.5 cm maximum particle size) weathered for 20-40 weeks in laboratory controlled conditions (Hirsche et al. (2017)). 1 liter of water was added at every weekly cycle, generating leachates with neutral pH.

- Field barrels: 6 kinetic tests each consisting of 350 kg of waste rock (max particle size 15cm) weathered for $\geq$ 10 years in field conditions (Vriens et al., 2019b; St-Arnault et al., 2020). Approximately 1500 liters of water were added over 10 years exhibiting a wide range of leachate quality.

- Composite laboratory column: 170 kg of mixed-composition waste rock (max particle size: 8 cm), weathered for one year in laboratory conditions; (Blackmore et al., 2014, 2018b).180 liters of water were added over one cycle, corresponding to the field barrel condition, generating a low-pH and low-quality drainage.

- Mesoscale instrumented waste-rock piles: 20 000 tons of mixed-composition waste rock (max particle size $\approx$ 1 m), weathered for over 10 years in the field (Vriens et al., 2019a), (Vriens et al., 2019c). Only the frontal tipping phases of these piles (described in prior publications as lysimeters C) were considered for modelling efforts. These experiments can be conceived of as 2 m x 2 m x 11 m columns ($\sim$100,000 kg of rock) embedded within the 36 m x 36 m x 11 m high experimental piles (Blackmore et al., 2014; Vriens et al., 2019a). Neutral and low quality leachates were observed depending on the waste rock lithology and mineral composition.

The particularly wide range of waste-rock lithologies produced at Antamina is divided into reactivity classes based on sulfide and metal content (Bay et al., 2009). We examine reactive (Antamina type A) **i**ntrusive (I) and **s**karn (S) rocks and slightly reactive (Antamina type B) **h**ornfels (H) and **m**arble (M) (see Tables S2 and S3 for particle size distribution and mineral contents). For this work, experiments were selected such that all major waste-rock lithologies were included in the analyses. Nomenclature of the investigated experiments is adopted from the works cited above. Measured bulk waste-rock properties in the investigated experiments include hydraulic parameters (porosity, hydraulic conductivity and van Genuchten parameters, Table S1; particle size distribution, Table S2), mineralogical data (Table S3) and elemental composition (Table S4). Drainage outflow and chemistry samples were collected on a weekly to monthly basis for the various experimental scales (Blackmore et al., 2018b; Vriens et al., 2019a,b,c).

2.2. Reactive transport modelling

2.2.1. Formulation

Reactive transport models were built in MIN3P-HPC (Mayer et al., 2002; Mayer and MacQuarrie, 2010; Su et al., 2017), which has been used for several studies involving mine waste drainage simulations (Mayer et al., 1999; Brookfield et al., 2006; Bea et al., 2012; Wilson et al., 2018). The code is used to model transient unsaturated flow, advective-diffusive-dispersive solute transport, gaseous diffusion, as well as the solid-liquid-gas equilibrium and kinetic reactions. Formulation of transient unsaturated flow follows Richards equation, in the form given in (Mayer et al., 2002):

$$S^l S_s \frac{\partial h}{\partial t} + \phi \frac{\partial S^l}{\partial t} - \overrightarrow{\nabla} \cdot \left[k_r^l K \overrightarrow{\nabla} h \right] = 0, \tag{1}$$

where k_r^l is the liquid relative permeability [-], K is the hydraulic conductivity [m·s^{-1}], h is the hydraulic head [m], S^l is the liquid saturation related to the volumetric water content θ through the porosity ϕ and S_s is the specific storage coefficient [m^{-1}]. Van Genuchten relations (Wösten and Van Genuchten, 1988) are used to compute the relative permeability and linkage between liquid saturation and hydraulic head (see SI).

All experiments were simulated as uniform 1D vertical flow systems where downward infiltration dominated the flow regime. Due to their limited heterogeneity and spatial scale (i.e. limited lateral flow dispersion), one-dimensional vertical models are suited to describe the smaller-scale experiments (humidity cells, field barrels and laboratory column), as was shown by previous studies (Wilson et al., 2018; Pabst et al., 2017). As larger-scale piles usually display more heterogeneous flow, dual-porosity and dual-permeability description might be more suited to capture preferential flow phenomena and short-term drainage dynamics. However, dual-domain formulations require additional parameters (e.g., inter-domain exchange terms) that are challenging to constrain experimentally (Arora et al., 2011; Moreira et al., 2016). Additionally, the impact of dual-domain dynamics on mass loadings over a yearly timescale is unclear. As will be shown below, a uniform flow formulation was considered satisfactory for the purpose of this study, which is to focus on the long-term trends in the drainage geochemistry. The mesoscale experimental piles represent a possibility to assess the capability of simplified model formulations to reproduce and predict long-term drainage dynamics on larger scales (Vriens et al., 2020).

Initial conditions for the unsaturated flow problem are constrained by volumetric water contents that were measured in the composite laboratory column as well as in the experimental piles; representative average values were estimated for the field barrels. The transient infiltration rate (i.e. precipitation - evapotranspiration) at the top boundary and a constant volumetric water content at the bottom were selected to match observed outflow rates. The humidity-cell experimental wetting-drying cycles (complete saturation followed by gradual drying) were mimicked by an averaged "continuous flow" that produced the same total water flux.

Transport of solutes and gaseous species, and the solid-liquid-gas equilibrium is modeled as:

$$\frac{\partial \phi S^l T_i^l}{\partial t} + \frac{\partial \phi S^g T_i^g}{\partial t} = \overrightarrow{\nabla} \cdot \left[\phi S^g \boldsymbol{D^g} \overrightarrow{\nabla} T_i^g + \phi S^l \boldsymbol{D^l} \overrightarrow{\nabla} T_i^l - T_i^l \overrightarrow{u} \right] + R_i^{\min}, \quad (2)$$

where S^g is the gas saturation, T_i^l and T_i^g respectively are the total concentrations of basis species i in the aqueous [mol $\cdot$ L^{-1}of water] and gaseous [mol $\cdot$ L^{-1}of gas] phases, u is the Darcy-velocity [m.s^{-1}]. $\boldsymbol{D^l}$ and $\boldsymbol{D^g}$ represent the liquid and gas diffusion-dispersion tensors [m^2 $\cdot$ s^{-1}], assumed isotropic:

$$\begin{cases} \boldsymbol{D^l} &= \delta |\overrightarrow{u}| + D_0^l \\ \boldsymbol{D^g} &= D_0^g \end{cases}, \quad (3)$$

where δ is the dispersivity [m] and D_0^l, D_0^g are the pore diffusion coefficients [m^2 $\cdot$ s^{-1}] (Table S1). $R_i^{\min}$ represent the source-sink terms from the mineral reactions [mol $\cdot$ dm$_{\text{bulk}}^{-3}\cdot$ s^{-1}]. In all simulations, infiltrating and pore solutions were initially in equilibrium with atmospheric oxygen (20% partial pressure) and carbon dioxide (0.04 %), corrected for the prevailing atmospheric pressure at Antamina; ∼4,400 m above sea level. Gas partial pressures are maintained constant at the top of the domain, while a free exit is modeled at the bottom boundary.

The different models described a 2cm grid cells, except for the experimental pile which was modeled using a coarser mesh (10 cm). Convergence is reached when the maximum concentration relative evolution between two successive iterations (over every species and every node) is below 10^{-6}. Convergence is assumed to not be reached above a certain number of Newton-Raphson iteration, after which MIN3P reduces the timestep. Also, when the solver requires more than 12 iterations, timestep is reduced. The maximum allowed timestep was set to 12h.

2.2.2. Geochemical reactions

Major minerals present in the waste rocks (Table S3) include the sulfide minerals, pyrite, chalcopyrite, sphalerite, molybdenite and galena. Other (non-sulfide) primary phases included calcite and silicate minerals, biotite, albite, quartz, anorthite, muscovite and wollastonite. Based on previous observations, the following secondary minerals were considered: gypsum, ferrihydrite, powellite (Conlan et al., 2012), amorphous silica and aluminum, wulfenite, jarosite, willemite (Skierszkan et al., 2016), as well as several Cu/Zn-(oxyhydr)oxides, sulfates and carbonates (Vriens et al., 2019a). The considered minerals are summarized up in Table S5 and their rate expressions are given in Table S6. We distinguished between quasi-equilibrium and kinetic rate expressions for fast and reversible versus slower and irreversible dissolution reactions, respectively. Reversible and fast reactions can effectively be described by generalized transition state theory rate expressions (Mayer et al., 2002; Lasaga and Kirkpatrick, 2018), with Q_m and K_m representing respectively the ion activity product and the thermodynamic equilibrium constant and k_{eff} the rate constant (in mol . $\text{dm}^{-3}_{\text{bulk}}$. s^{-1}) :

$$R_m = k_{\text{eff}} \left(1 - \frac{Q_m}{K_m}\right) \tag{4}$$

For large rate coefficients, this equation yields quasi-equilibrium conditions, if the mineral phase in question is present. Aqueous and gaseous equilibrium constants, as well as aqueous speciation chemistry constants were adopted from the MINTEQ.v4 database.

Irreversible, slower mineral dissolution reactions were described by kinetic rate expressions adopted from the literature. Rate laws for sulfide and silicate minerals have been widely studied (e.g., Rimstidt et al. (1994)). All rate laws depend upon the experimental conditions and literature rate expressions are usually contain surface-area normalized rate constants in $\text{mol.m}^{-2}\text{.s}^{-1}$, and were corrected by what will be referred to as the reactive surface area A_{eff} (in $\text{m}^2\text{.dm}^{-3}_{\text{bulk}}$). To capture sulfide oxidation by dissolved oxygen and ferric ion (Singer and Stumm, 1970) in a single rate expression, the pyrite and sphalerite rate laws were adapted from Williamson and Rimstidt (1994) and Pan et al. (2012), respectively, in the forms:

$$R_{\text{pyrite}} = A^{\text{Py}}_{\text{eff}} \left(10^{-8.19} \frac{[O_2(\text{aq})]^{0.5}}{[H^+]^{0.11}} + 10^{-6.07} \frac{\left[\text{Fe}^{3+}\right]^{0.93}}{\left[\text{Fe}^{2+}\right]^{0.4}}\right) \tag{5}$$

$$R_{\text{sphalerite}} = A_{\text{eff}}^{\text{sph}} \left(10^{1.163} \left[H^+\right]^{0.11} \left[\text{Fe}^{3+}\right]^{0.154} \right) \quad (6)$$

For chalcopyrite, rate laws reported by Salazar et al. (2009) ,Rimstidt et al. (1994) and Kimball et al. (2010) were mostly developed under acidic conditions ($1 \leq \text{pH} \leq 3$) not representative of the wide range of drainage conditions encountered in our experiments ($2 \leq \text{pH} \leq 9$). Furthermore, chalcopyrite rate laws for $\text{pH} \leq 3$ exhibited a high-order dependence on pH ($\left[\text{H}^+\right]^{1.68}$). Considering the progressive acidification of over 5 pH units observed in some Antamina experiments, use of such a law would yield oxidation rates increasing by over 8 orders of magnitude. Therefore, the oxidation of chalcopyrite, but also that of molybdenite and galena, was described by a simple first-order dependence on dissolved oxygen:

$$R_{\text{chalcopyrite}} = A_{\text{eff}}^{\text{Chalco}} \left[\text{O}_2(\text{aq})\right], \quad (7)$$

Literature-adopted kinetic rate expressions for all considered sulfide and silicate phases are summarized in Table 1.

Table 1: Kinetic formulations for the mineral rates. Thermodynamic constants were taken from the MINTEQ database

Mineral	**Rate expression** R_m	
Pyrite	$A_{\text{eff}}^{\text{Py}}(10^{-8.19}\frac{[O_2(\text{aq})]^{0.5}}{[H^+]^{0.11}}+10^{-6.07}\frac{\left[\text{Fe}^{3+}\right]^{0.93}}{\left[\text{Fe}^{2+}\right]^{0.4}})$	Williamson and Rimstidt (1994)
Sphalerite	$A_{\text{eff}}^{\text{sph}}\left(10^{1.163}\left[H^+\right]^{0.11}\left[\text{Fe}^{3+}\right]^{0.154}\right)$	Pan et al. (2012)
Chalcopyrite Molybdenite Galena	$A_{\text{eff}}^{\text{m}}\left[O_2(\text{aq})\right]$	
Quartz	$A_{\text{eff}}^{\text{Qu}}(10^{-12}+10^{-13.8}[H^+]^{-0.25})$	Dove (1995)
Albite	$A_{\text{eff}}^{\text{Alb}}(10^{-9.69}[H^+]^{0.49}+10^{-14.15}[H^+]^{-0.3})$	Chou and Wollast (1985)
Biotite	$A_{\text{eff}}^{\text{Bio}}\left[H^+\right]^{0.25}$	Acker and Bricker (1992); Bray et al. (2015)
Anorthite	$A_{\text{eff}}^{\text{An}}(10^{-5.87}[H^+]^{1.12})$	Brady and Walther (1989)
Muscovite	$A_{\text{eff}}^{\text{Mu}}(10^{-12.6}[H^+]^{0.08}+10^{-13.5}[H^+]^{-0.1})$	Nickel (1973)
Others	$k_{\text{eff}}^{\text{m}}\left(\frac{Q_{\text{m}}}{K_{\text{m}}}-1\right)$	

2.3. Model parametrization and calibration

The reactive transport formulation was applied consistently to the 15 investigated experiments. For all experiments, system geometry (Table S1), waste-rock bulk density and mineral abundance was measured and directly

adopted. Only identified minerals (Table S3) were considered to calibrate the initial mineralogy. For all experiments other than the humidity cells, hydraulic parameters (porosity, saturated hydraulic conductivity and van Genuchten parameters) were adopted from previous tracer test analyses (summarized in Table S1). In all simulations, the sames values of dispersivity δ, specific-storage coefficient S_s and diffusivities D_0^g and D_0^l were used (Table S1). The only differences among the simulations of the various experiments were therefore i) initial and boundary conditions for flow (initial water content and recharge at the top boundary); and ii) effective mineral rate constants (k_{eff} ; Equation 4) and surface area (A_{eff} ; in Equations 5, 6 and 7) values as in Table S6.

For each simulation, calibration proceeded in two steps. First, initial head conditions for flow were set to be representative of the average observed water content. Volumetric water content and the recharge boundary conditions were calibrated to reproduce the observed outflow, except for the piles where recharge was calibrated to the observed weather record (Vriens et al., 2019a). Once hydraulics were calibrated and subsequently fixed, reactive surface area and effective rate coefficients (A_{eff} and k_{eff}) were adjusted to reproduce leachate concentrations in an informal trial-and-error fashion. Emphasis was placed on reproduction of long-term drainage concentrations, rather than initial spikes in the drainage concentrations arising from flushing of pre-experimentally precipitated salts. As such, A_{eff} and k_{eff} values represent the sole geochemical calibration factors and aggregate all influences of other unaccounted processes on the outflow chemistry, e.g., influence of temperature.

A number of hydrogeochemical feedbacks previously identified in mine waste-rock systems - including Antamina - were not explicitly incorporated in the model. These include, e.g., porosity and permeability changes through mineral precipitation (St.Arnault et al., 2019), gas advection (Amos et al., 2009; Vriens et al., 2018), preferential flow (Stockwell et al., 2006; Trinchero et al., 2011; Lahmira et al., 2017; Appels et al., 2018; Blackmore et al., 2018a), surface passivation and reactive surface area decreases (e.g., 'shrinking core model' Wunderly et al. (1996); Langman et al. (2014); St.Arnault et al. (2019)), microbial catalysis (Blackmore et al., 2018b) or chemical adsorption (Vriens et al., 2019b). In some cases, the exclusion of these processes is justified by experimental data, e.g., limited O_2 depletion and heat production to support convection). Porosity changes fall in the same category: simulated changes in the volumes of mineral phases were small (less

than 10% for the most reactive waste rock). The exclusion of other processes (e.g., preferential flow and evolution of reactivity) could not be justified from experimental evidence, but limited or no data was available to support their parametrization across the investigated experiments. Hence, these processes were not considered in line with our approach to develop a model "as simple as possible, as complicated as necessary" and the effects of these unresolved processes are integrated by the fitted geochemical rate constants. A quantitative analysis of these unresolved contributions is the primary focus of Vriens et al. (2020), while this study examines the ability of the model formulation and individual considered processes to capture long-term drainage dynamics across experimental scales.

2.4. Sensitivity analyses

Individual processes and feedbacks were investigated through a sequence of sensitivity analyses run on calibrated simulation models. Specifically, we considered the role of secondary mineral reaction rates (sensitivity on k_{eff}), evolution of reactive surface area (temporal evolution of A_{eff}) and the influence of hydraulic parameters and volumetric water content on drainage dynamics. Details and results of these sensitivity analyses can be found in the SI.

3. Results and Discussion

3.1. Humidity cells

The humidity-cell tests contained relatively homogeneous sieved waste rock with narrow particle size distributions and displayed no drainage acidification during the short term (up to 40 weeks) they were run. The simulated compositions in all investigated humidity-cell experiments are in good agreement with measured compositions (Figure 1).

In all humidity-cell experiments, neutral-drainage pH was observed. Simulations suggest that this is because of a stoichiometrically balanced sulfide oxidation and calcite dissolution, whose rates were approximately 10^{-5} mol $\text{dm}_{\text{bulk}}^{-3}\text{day}^{-1}$across waste rock types (Figure 2). These reasonable weathering rates suggest that no significant oxygen limitation occurs within the one-week wetting cycles. Calibrated pyrite reactive surface area and calcite effective rate coefficients varied less than a factor 4 between all the investigated experiments (Table S6).

Humidity-cell experiments are designed to examine whether the AP/NP balance affects the ultimate acidity and composition of drainage when all potential weathering products are mobilized. As such, humidity cells are assumed to not reach mineral saturation (Sapsford et al., 2009; Maest and Nordstrom, 2017). Yet, simulations reveal that some secondary mineral phases were close to saturation (SI > -1: Figure 2). Precipitation of secondary Fe-(oxyhydr)oxides, generalized as ferrihydrite in the model, and a copper hydroxide ($Cu(OH)_2$, tenorite in the MINTEQ database) induced below detection limits concentrations of Fe and Cu in the drainage respectively. Simulations suggest that $\sim$ 50-150 mg/kg of ferrihydrite (1-3 mmol over the 2kg waste rock) precipitated by the end of each humidity-cell experiment. Low drainage concentrations of Zn are primarily due to low Zn abundance (except for HC5) and the circumneutral pH which does not promote sphalerite oxidation (Equation 6). Other (near)saturated secondary mineral phases included wulfenite, whose precipitation attenuates Mo, as shown for humidity cell HC1 in Figure 1 and 2. The simulated low cumulative precipitation of these secondary phases through time (Figure 2) indicates that these minerals would not be readily detectable with conventional mineralogical techniques.

Humidity-cell experiments with skarn and intrusive waste rock released significant Ca and sulfate during the first $\sim$20 days, possibly related to the dissolution of secondary gypsum that had precipitated on the waste rock prior to the start of the kinetic tests. Indeed, inclusion of a small amount of gypsum (0.02 % volume fraction) to the mineral assemblage led to a better representation of the observed "first flush" (dashed red-line in Figure 1) but was not further adopted in other simulations to ensure consistency across experiments.

3.2. Field barrels

Compared to the humidity cells, field-barrel experiments contained greater than two orders-of-magnitude more waste rock and were run more than 10 times longer, for 9 years, and under field conditions. A wide range of drainage signatures was observed in the suite of field barrels, ranging from metastable, seasonally oscillating, circumneutral drainage to gradually acidifying drainage with orders-of-magnitude increases in metal loads (Figure 3). Simulated drainage chemistries reproduce observed values for all investigated waste-rock types (Figure 3 and additional field barrels in Figure S3), including an accurate representation of temporal oscillation in drainage quality and quantity.

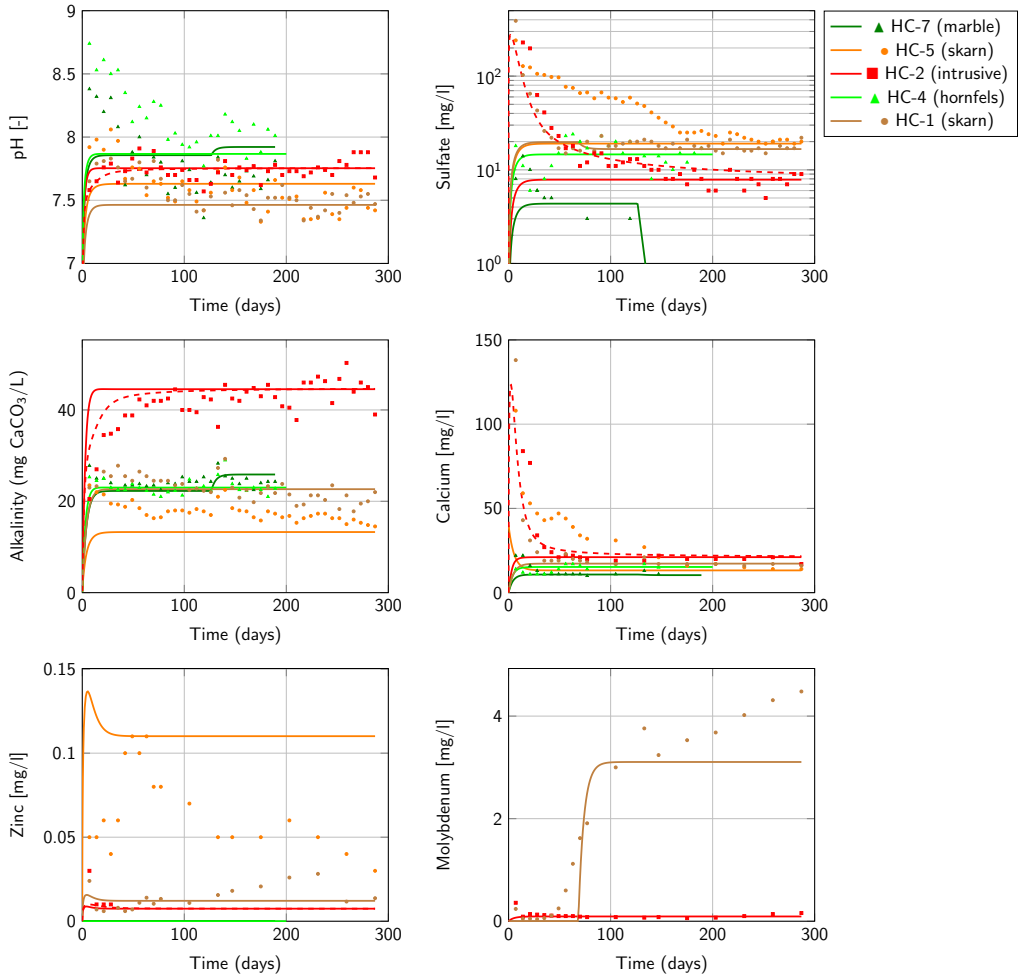

Figure 1: Recorded and simulated drainage chemistry for humidity test cells. Drainage pH, alkalinity, Ca and sulfate concentrations (logarithmic y-axis for the latter) are plotted for experiments and simulations that are color-coded based on their lithology. Solid lines indicate model results while markers indicate measured values. Mo concentrations are only displayed when they were above detection limits (HC-1 and HC-2 only). The red dashed line corresponds to the HC-2 simulation with an initial small amount of gypsum, whose rate decreases exponentially, using equation S2.

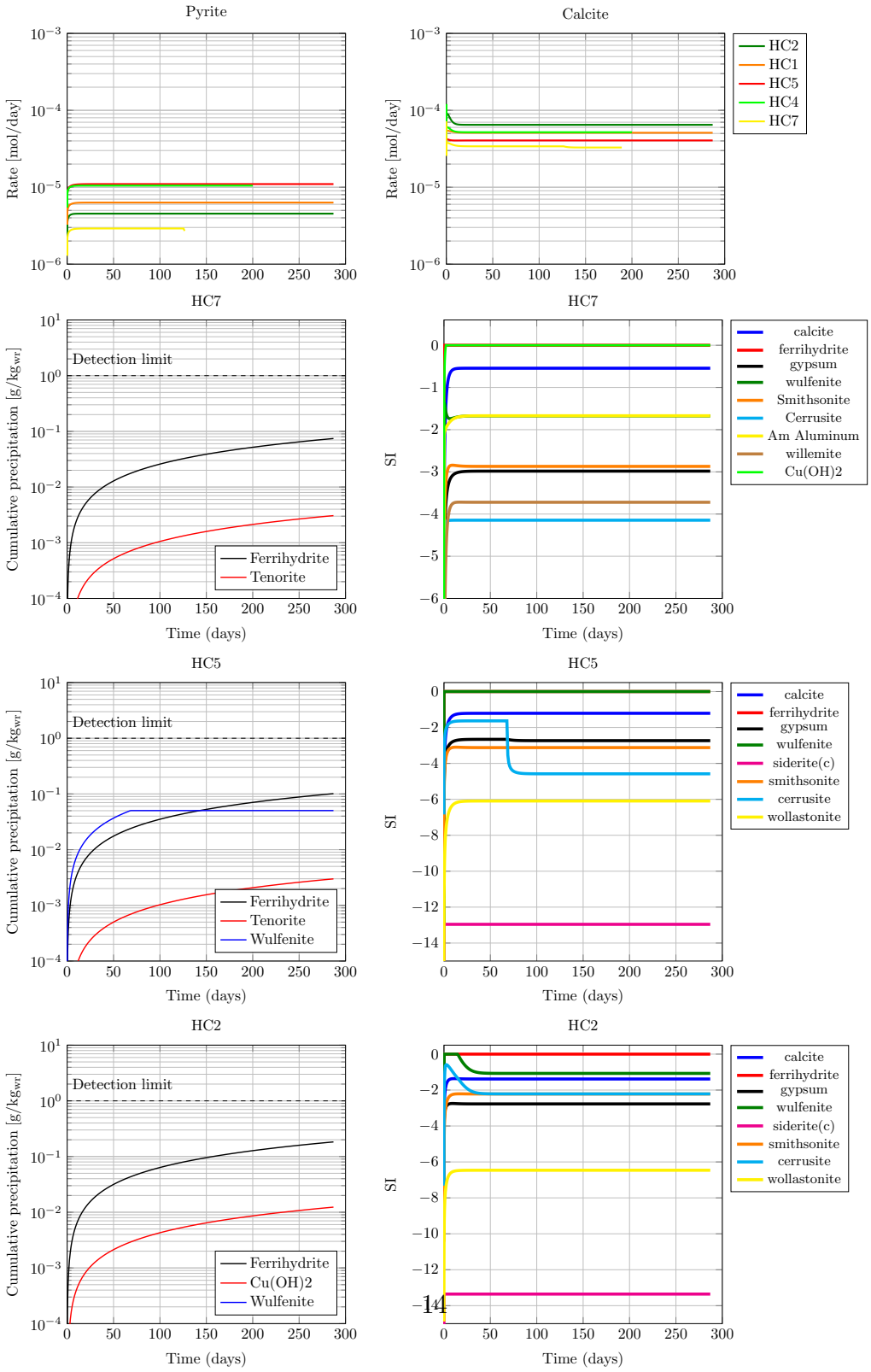

Figure 2: Top: Simulated rates of pyrite oxidation and calcite dissolution. Middle: evolution of secondary mineral precipitation for the three most reactive humidity cells, compared to typical XRD detection limit of 0.1 wt-%. Bottom: saturation indices (SI) of a series of

Simulated volumetric water content and oxygen profiles can be found in Figure S2. The seasonal variation in flow rates simulated for the field barrel experiments (Figure S1) affect the temporal evolution in simulated drainage chemistry (Figure 3): elevated infiltration during the wet season increases the waste-rock water content and dilutes solutes. Simulated mineral dissolution rates (e.g., R_{pyrite} from Equation 5) also oscillate in time (Figure 4), potentially due to the evolution of the air-filled porosity that impacts oxygen supply to the waste rock in the field-barrels. Simulations indicate that oxygen levels generally remain very close to atmospheric levels (Figure S2), with a minimum oxygen content of 70% compared to ambient conditions, even for the most reactive field-barrel. Even though oxygen depletion was therefore probably limited, simulations suggest that small variations in oxygen and water content still impact sulfide oxidation rates through the evolution of ferrous and ferric iron concentrations (Equation 5). Coarser-grained materials like FB-M1 (Table S2) are drier (Figure S2), less reactive and therefore have a rather constant oxygen profile (Figure S2) and stable oxidation rates (Figure 4), compared to finer-grained and more reactive materials (FB-S4 or FB-I9). Also, calcite weathering rates seem to be strongly correlated to the volumetric water content, even for low-reactivity field barrel with steady oxidation rates (FB-M1 on Figure 4). This is further confirmed by sensitivity analysis (Figure S7).

Field barrels FB-I2 (intrusive), FB-S1 and FB-S4 (skarn), FB-H1 (hornfels) and FB-M1 (marble) remained circumneutral for the $\geq$10-year study period. However, drainage from field barrel FB-I9 (intrusive) transitioned from $\sim$ 6.5 to pH $\leq$ 3 within 3 years, associated with orders-of-magnitude increasing concentrations of sulfate, Cu and Zn (Figure 3). Simulations show that this acidification was caused by depletion of calcite initially present in the field barrel ($\leq$0.1 wt-%, see Table S3) within the first two years (Figure 4). The absence of buffering by calcite initiated a feedback where pyrite and sphalerite oxidations was accelerated through the decreasing pH and increasing ferric iron concentration (Equations 5 and 6; Figure 4). The model was able to capture such rate increases without adjustments to the fitted rate parameters, because the rate expressions explicitly accounted for pH and dissolved iron concentrations (Equations 5 and 6). Simulations show that acid was buffered in FB-I9 principally by dissolution of amorphous Fe-oxides (Ferrihydrite in Figure 4 dissolves after 4 years), and subsequently by dissolution of silicate phases such as wollastonite, present at $\geq$2 wt-% in FB-I9 (Table S3), albite and biotite (Figure 4). This sequence of mineral dissolution under

increasingly acidic conditions reflects a typical acid-rock drainage neutralization series (Sherlock et al., 1995; Amos et al., 2015; Vriens et al., 2019a).

A number of secondary mineral phases identified in the field-barrel experiments by St.Arnault et al. (2019) and Vriens et al. (2019b) were near saturation in the simulation, including gypsum, various Fe-, Cu-(oxyhydr)oxides and Cu-(hydroxy)sulfates, as well as willemite, wulfenite and powellite (as shown through their precipitation depicted in Figure 4). This supports the notion that significant metal attenuation takes place under neutral drainage conditions. For instance, simulations suggest that $\sim$ 1 mole of secondary Cu-hydroxy-sulfates ($\sim$ 450 grams of brochantite and $\sim$ 350 grams of antlerite over the 350 kg waste rock) precipitated in field barrel FB-I9 during the first 4 years (Figure 4), with a conversion from brochantite to antlerite. Once acidic conditions developed within FB-I9, both these phases rapidly re-dissolved: the net effect of this re-dissolution coupled to the ongoing chalcopyrite oxidation explains the Cu mobilization spike observed after 2 years (Figure 3). Moreover, precipitation of jarosite ($\sim$ 1.4 g/kg of waste rock) acts to attenuate Fe as ferrihydrite starts to dissolve under acidic pH (Figure 4). Typically, simulated drainage composition was highly sensitive to the secondary mineral assemblage, as illustrated by the effect of the ferrihydrite reaction rate illustrated by a sensitivity analysis (Figure S5 in SI): the limit case where ferrihydrite is inert (or not included in the model), induces more acidic conditions in the drainage, with a positive feedback on oxidation rates of primary minerals and therefore the overall sulfate loading. These examples demonstrate the value of modeling to help identify secondary-mineral controls that, because of their low abundances or amorphicity, would be challenging to determine experimentally in heterogeneous weathered waste rock.

There are other explanations for the limited buffering capacity of field barrel FB-I9: a progressive passivation through secondary mineral precipitation (e.g., St.Arnault et al. (2019)), or a reactivity decrease caused by preferential weathering of finer-calcite grains (Beckingham et al., 2016; Seigneur et al., 2019). As shown in the sensitivity analysis in the SI (Figure S6), a better agreement between simulated and measured Ca concentrations can be obtained by progressively reducing calcite reactivity (k_{eff}) during dissolution. The shrinking core model (Ritchie, 1994; Levenspiel, 1998), or other approaches (e.g., Jeen et al. (2007)) to model the impact of precipitation on the decrease in reactivity could be considered to address decreasing mineral reactivity over the course of weathering. However, these approaches may also lack in experimental evidence to be properly parametrized (e.g., the thickness

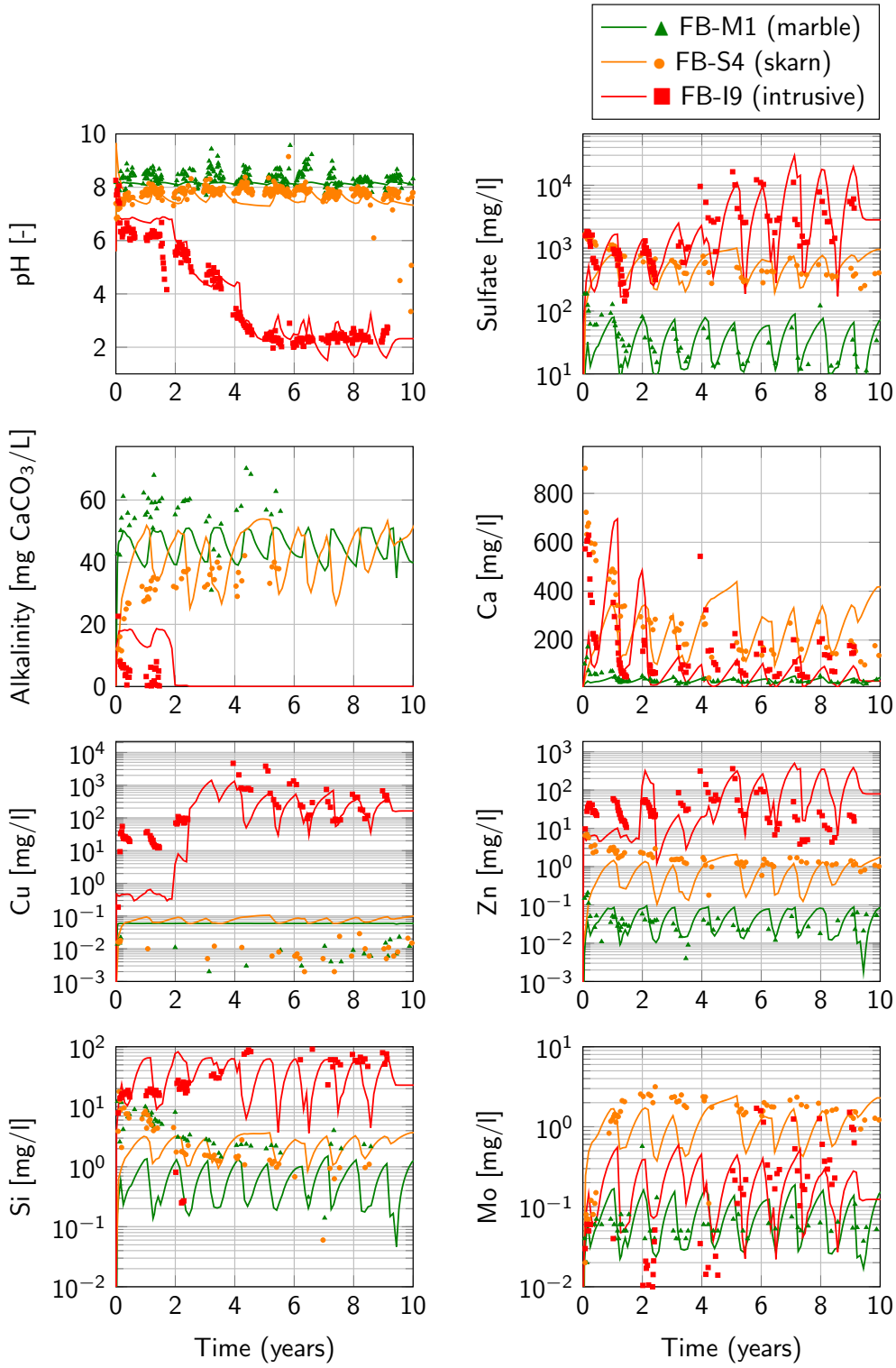

Figure 3: Observed and simulated drainage chemistry for the field barrels. Experiments and simulations are color-coded by their lithology and show drainage pH, alkalinity and aqueous concentrations of Ca, Si, Mo (linear y-axis) as well as sulfate, Cu and Zn (all logarithmic y-axes). Legend applies to all frames. Solid lines indicate model results while markers indicate measured values. Results for additional experiments FB-I2 (intrusive), FB-H1 (hornfels) and FB-S1 (skarn) are given in Figure S3

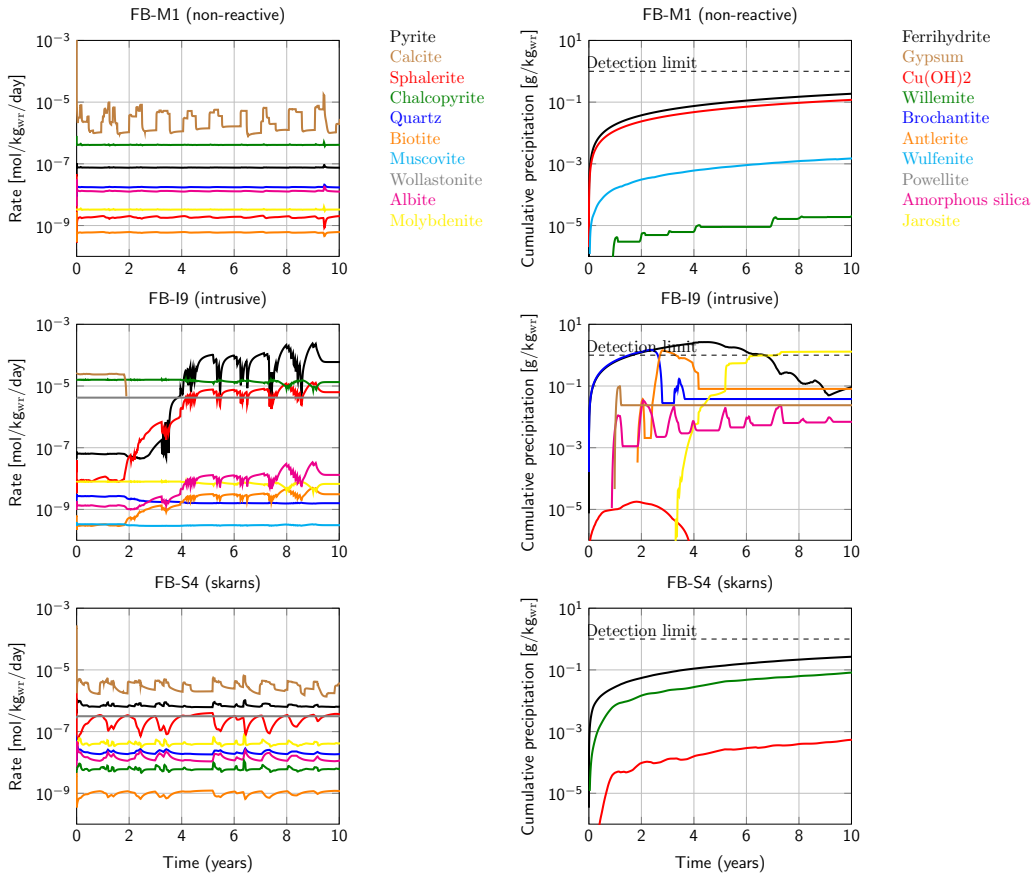

Figure 4: Simulated rates of primary mineral dissolution (left column) and cumulative precipitation of secondary minerals (right) in the three field barrel experiments presented in Figure 3. Simulated precipitation of secondary minerals are compared to a typical XRD detection limit of 0.1 wt-%

and diffusivity of reactive rim).

That we are able to capture the essential solute mobilization dynamics from materials subject to field conditions displaying variable geochemical drainage conditions ($2 \leq \text{pH} \leq 9$), with different hydraulic behavior and geochemical properties which can be a-priori estimated based on bulk-average characterization of the waste-rock systems, demonstrates the robustness of our modelling approach.

The fitted pyrite reactive surface areas used in the field-barrel simulations varied from each other with less than one order-of-magnitude, and were generally two orders-of-magnitude lower than those used in the humidity cells simulations (Table S6). This difference is associated to the coarser-grained rock and the effects of lower ambient temperature in the field barrels (Vriens et al., 2020). The fitted pyrite reactive surface area for waste rock in FB-I9 was lower than for FB-I2, a similar reactive, instrusive waste rock, but with relatively larger grain size (Table S2). A strong correlation exists between the physical surface areas deduced from particle size distributions and fitted reactive surface areas (Vriens et al., 2020). Despite a lower surface area, acid generation in FB-I9 results from the low carbonate (Table S1) and high chalcopyrite (Tables S3 and S4) contents.

3.3. Composite laboratory column

Although similar in size to the field barrels and of shorter duration, the laboratory column experiment added complexity because it was composed of three different waste rock types that were vertically stacked: the bottom drainage carried the aggregate signal of all waste-rock types. Yet, observed drainage rates and internal moisture-content profiles (Figure S1 and top right of Figure 6, respectively) could be well captured by our model using unadjusted hydraulic properties that were fixed for each waste-rock layer.

Simulated drainage chemistries generally agree with observations as well (Figure 5). The initial important flush of oxidation product (observed for many elements; Figure 5) is because of the progressive build-up occurring during the wetting-up of the column (the first 120 days where no outflow occurred) and can be observed from the element concentration profiles (Figure 6).

The laboratory column experiment produced basal drainage that was mildly acidic ($4.5 \leq \text{pH} \leq 5$); drainage was not sampled from within the column from the individual waste-rock layers. The simulated outflow chemistry matched that of the outflow when acidity was simulated as mostly produced

in the uppermost layers that contained reactive waste rock with high sulfide content (up to 6 wt-%, Table S3), and low NP/AP ratios, at rates of up to 10^{-5} mol $dm^{-3}_{bulk}day^{-1}$(see Figure S4). Local porewater pH in the uppermost column layers dropped to pH $\leq$ 2.5, while sulfide oxidation and acidity production were negligible in the bottom marble rock. These sulfide oxidation rates are comparable to those simulated for field barrels with similarly reactive waste rock (e.g., up to 10^{-5} mol $dm^{-3}_{bulk}day^{-1}$FB-I9, Figure 4). Simulated pyrite reactive surface areas for the column top layer were higher those used in the field barrels but lower than the humidity cells.

The simulations suggest that wollastonite, which was identified in the central part of the column (Table S3), is the primary buffering phase in the more reactive waste rock segments ($\sim 10^{-5}$ mol $dm^{-3}_{bulk}day^{-1}$, see Figure S4). Several mineral phases were saturated in the top waste-rock layers (Figure 6), e.g., amorphous Silica and Fe-oxides, as well as jarosite and Cu-(hydroxy)sulfate phases. These are the same mineral phases important to obtain a quantitative agreement between measured and simulated (acidic) drainage of field-barrel FB-I9 (which had waste rock similar to that in the top layers in the laboratory column) our reactive transport framework therefore suggests that incorporation of these phases is important for simulating acid rock drainage.

The fact that the composite column drainage had a pH$\leq$5 implies that neutralization of acidic drainage percolating from the uppermost layers in the lower marble layer was not very effective. This is surprising considering that the bottom marble layer consisted virtually exclusively of carbonates and silicates (up to 75 wt-% calcite, Table S3). The ineffective neutralization can be explained by smaller relative surface areas (coarse grains within this layer, see Table S2) and a shorter contact time with percolating drainage through flow channeling. Despite the observed limited neutralization, the drainage contains significant Ca ($\geq$ 500 mg/L), which cannot have been solely produced from wollastonite dissolution, as indicated by the low aqueous Si concentrations. As the drainage composition is in equilibrium with gypsum throughout the duration of the laboratory experiment (Figure 6), the slightly acidic pH and high Ca and sulfate concentrations likely are due to the dissolution of pre-existing gypsum, which formed during waste rock storage prior to the experimental period (Blackmore et al., 2018b). Pre-experimental gypsum could act as a passivation agent, reducing calcite dissolution during the experiment (St.Arnault et al., 2019). As only one single seasonal infiltration cycle was applied, these simulations depend strongly on the uncertain initial

(first flush) conditions. Further research over several pore volumes of infiltration is required to disentangle the roles of surface area passivation and flow channeling on the observed drainage dynamics.

3.4. Experimental piles

The experimental waste-rock piles are the largest experiments in the Antamina research program. While seasonal flow variability for the smaller-scale systems examined thus far could be quantitatively reproduced by the adopted uniform-flow description, seasonal variation in drainage rates from the larger experimental piles was significantly muted, even though cumulative long-term dynamics were well captured (Figure S1). This suggests that a uniform description may be valid for smaller-scale experiments with limited physical heterogeneity, but a single-domain flow description cannot reproduce seasonal oscillations at larger scales, because of the increased heterogeneity and contribution of preferential flow paths. This aligns with tracer test results from Antamina that have shown that matrix flow dominates transport at smaller scales, but that multi-domain flow formulations better capture solute dynamics from larger-scale experiments with strong contrasts in hydraulic properties (Blackmore et al., 2014; Pedretti et al., 2017), with fast flow amounting up to 15% of the total flow. Additional research would be required to study the representativity of our modelled mineral rates in a single continuum compared to the inherent nature of these multiple-continua, to investigate the potential of this approach to be integrated in even larger spatial scales.

While drainage from sublysimeter piles 1C and 3C remained neutral over the course of a decade, drainage in pile 2C acidified over several years (Figure 7), similar to what was observed for field barrel FB-I9: both systems consisted of reactive, sulfide-rich waste rock (Vriens et al., 2019a)). Oxygen distributions can be highly non-uniform throughout the piles (Vriens et al., 2019c). Even though no significant thermal gradients have been observed in the experimental piles, advective-driven supply of oxygen through the height of the pile is likely, especially near the atmospheric boundaries (Vriens et al., 2019c). Indeed, in large-scale waste-rock piles, the generally coarser particles and larger pores promote oxygen ingress by barometric (wind-driven) advection through the pile batters (Amos et al., 2009; Vriens et al., 2018, 2019c). Our simulation of pile 2C suggests that a purely diffusive flux from oxygen from the top boundary is not sufficient to maintain sulfide oxidation rates high enough to produce the measured sulfate concentrations in the

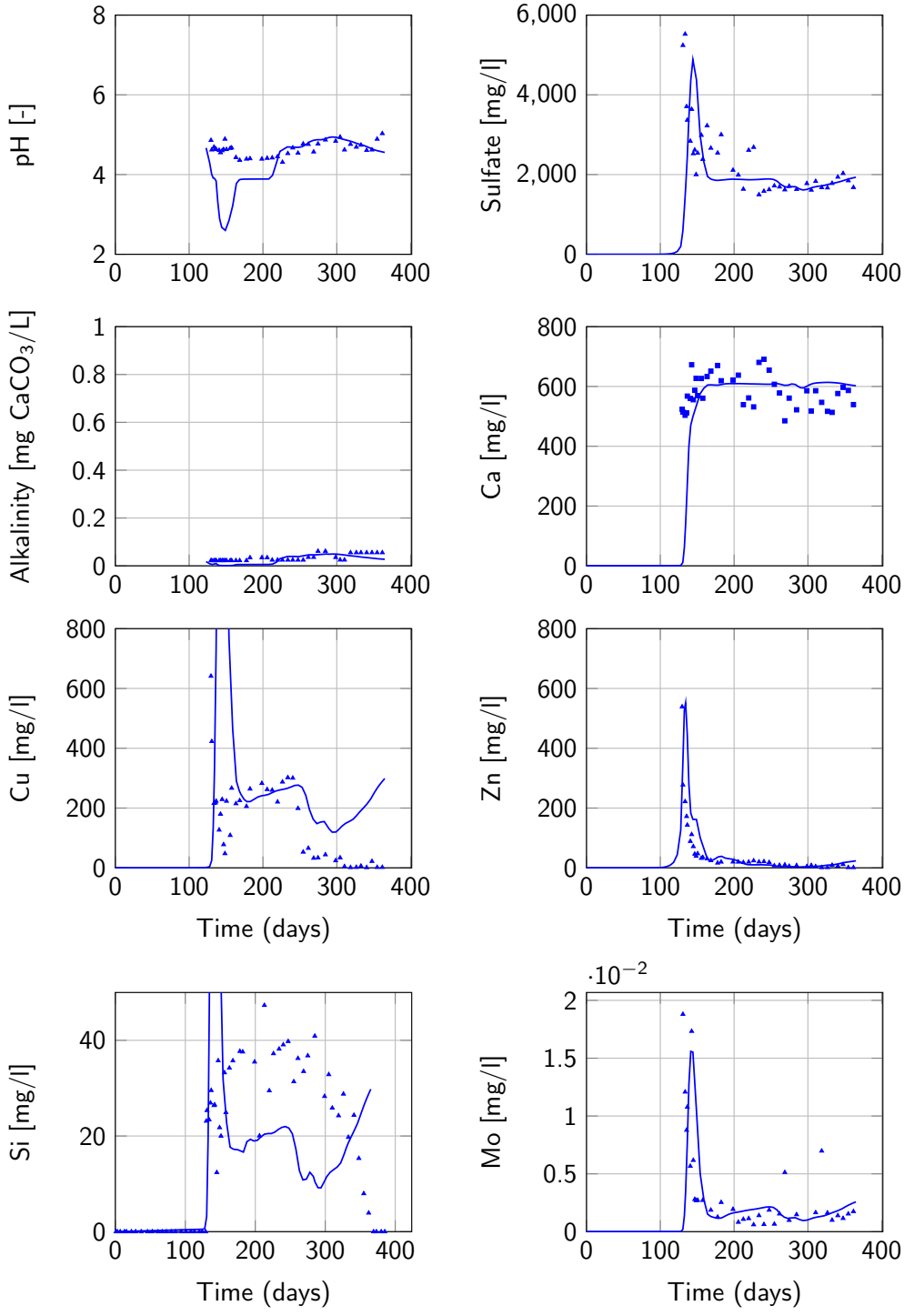

Figure 5: Observed and simulated basal drainage chemistry for the composite laboratory column for pH, alkalinity and aqueous concentrations of sulfate, Ca, Cu, Zn, Si and Mo.

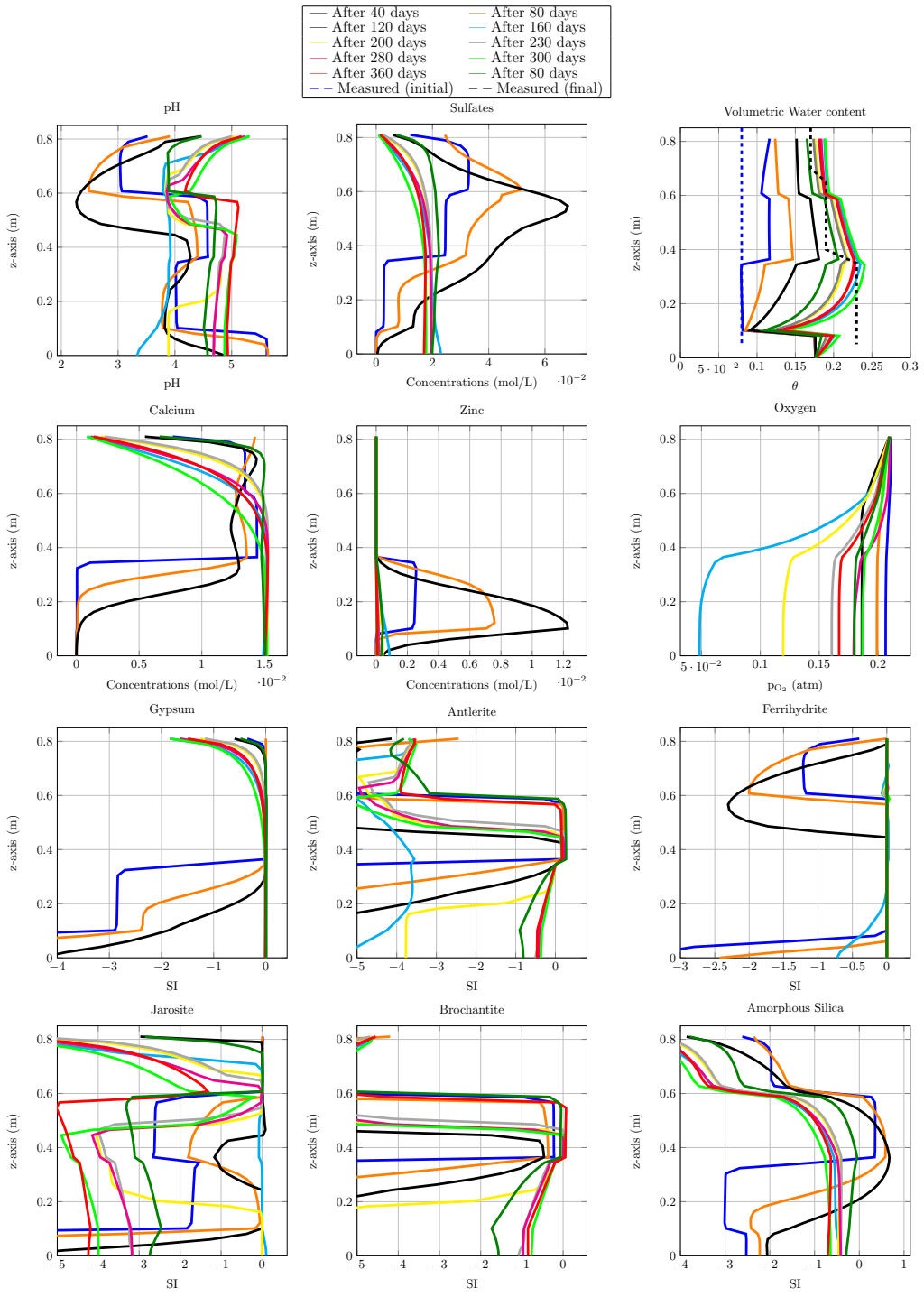

Figure 6: Depth-profiles of simulated solute concentrations and volumetric water content (upper two rows) and mineral saturation indices of selected mineral phases during the leaching of the composite laboratory column. No drainage exited the column until 120 days of weathering (Figure 5).

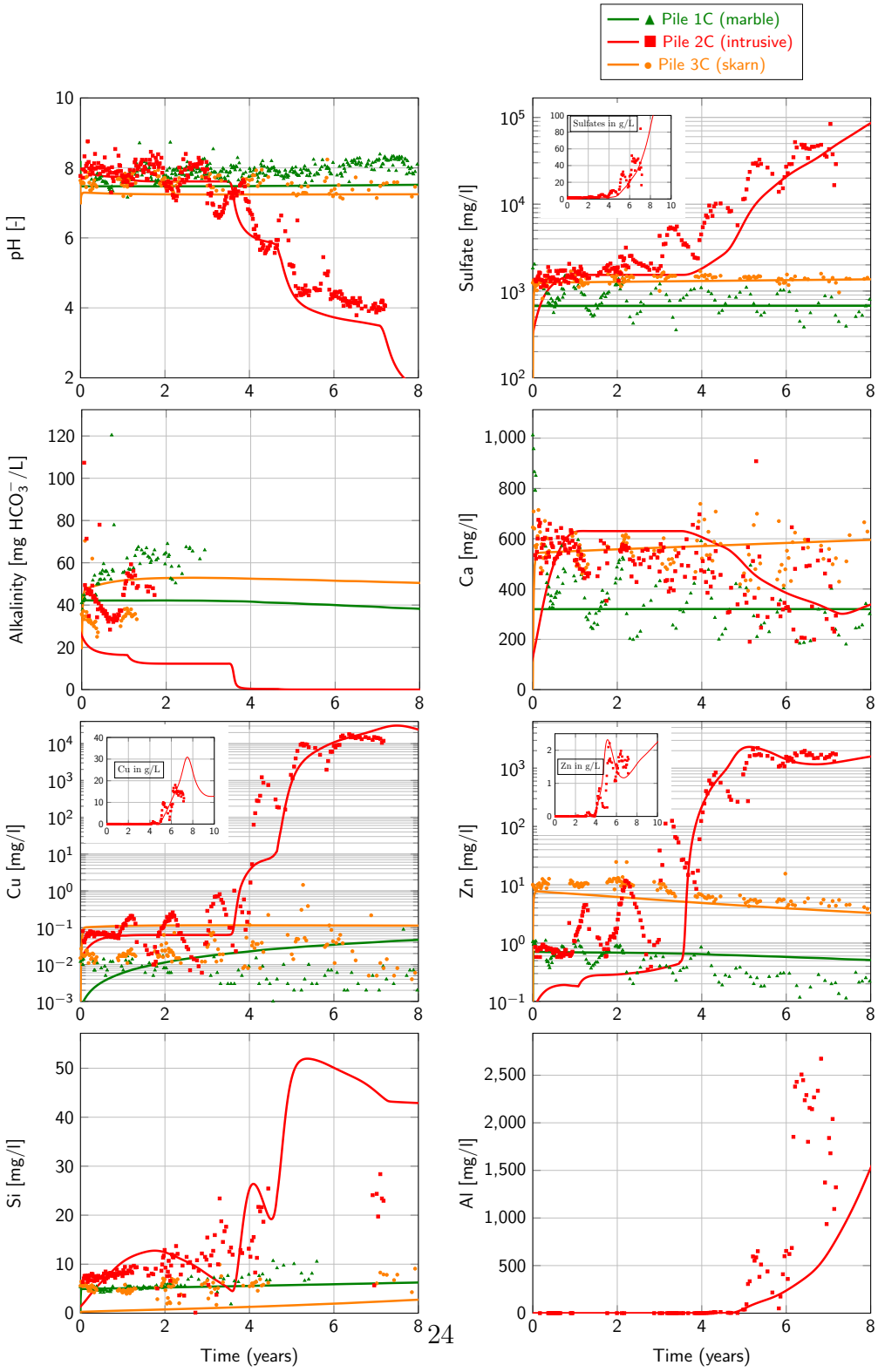

Figure 7: Measured and simulated drainage chemistry for lysimeter/tipping-phase C in experimental piles 1, 2 and 3 for pH, alkalinity and aqueous concentrations of Ca, sulfate, Cu and Zn (note logarithmic y-axes). The legend applies to all frames. Solid lines indicate model results while markers indicate measured values.

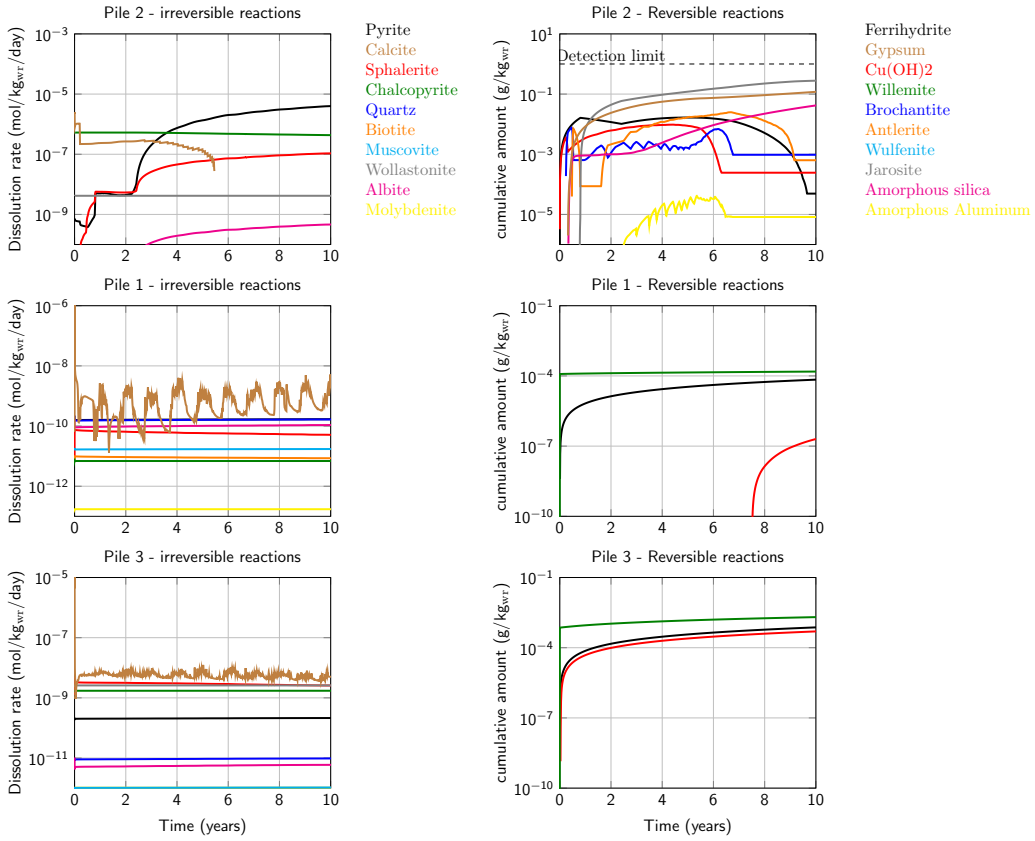

Figure 8: Simulated primary mineral dissolution rates (left column) and precipitated mass of selected secondary minerals (right column) during the weathering of the experimental piles. Simulated precipitation of secondary minerals are compared to a typical XRD detection limit of 0.1 wt-%

leachates ($\geq$ 50 g L^{-1}). This suggests that oxygen depletion is unlikely and that oxygen is supplied laterally through the pile batters by either diffusion and possibly advection. A lateral oxygen source is represented in the 1-D model as a constant oxygen pressure through the height of the pile 2C. Our adopted reactive transport framework and pile geometry do not explicitly include oxygen transport through sideward ingress into the piles. Therefore, the experimental waste-rock piles serve as a final test of the adopted one-dimensional uniform model formulation to reproduce waste-rock drainage dynamics at larger scales: the material in experimental pile 2C is similar to that in field barrel FB-I9 (Tables S3 and S4) and a quantitative comparison of reactive transport parameters between these two experiments can provide useful information regarding scale dependence of the adopted model (Vriens et al., 2020).

Simulated sulfide-oxidation rates in piles 1-3 varied between 10^{-9} and 10^{-6} mol $dm_{bulk}^{-3} day^{-1}$and align with bulk weathering rates that were experimentally determined from drainage loading rates, temperature profiles and *in-situ* poregas measurements, i.e. converted to molar units; 10^{-7} and 10^{-10} mol S $dm_{bulk}^{-3} day^{-1}$(Vriens et al., 2019a). Simulated pyrite reactive surface areas for the experimental piles were more than one order of magnitude lower compared to the field barrels. The reproduction of drainage acidification in pile 2C drainage was accompanied by acid-buffering dissolution of carbonate, Fe/Al-oxides, and silicate minerals (Figure 8) similar to the neutralization sequence described for FB-I9 above (Figure 4), with influence of Cu-sulfate (antlerite, brochantite) and jarosite. Additionally, simulated precipitation of secondary minerals aligned between simulations of FB-I9 and pile 2C (Figure 4 and Figure 8), with a general one order-of-magnitude lower cumulative precipitation.

Our reactive transport framework was able to simulate both FB-I9 and pile 2C, systems with same rock but on different scales, using similar geochemical factors (sulfide and silicate reactive surface areas and calcite effective rate constants; Table S6).

Finally, in all experimental piles, simulated drainage quality was strongly influenced by equilibria with calcite, ferrihydrite and gypsum (Figure 8). Simulated zinc concentrations were regulated by the precipitation/dissolution of willemite, a zinc silicate which has been previously identified at Antamina as a candidate for zinc attenuation (Skierszkan et al., 2016). The larger sizes of the waste-rock piles and higher average hydraulic residence time of $\sim$ 1 year in the piles - much longer than those in the smaller-scale experiments

investigated - allowed secondary minerals precipitates to larger extents. This yields a higher sensitivity to secondary mineral reaction rates compared to smaller-scale field barrel FB-I9 (Figure S5).

4. Conclusions

Reactive transport modelling of coupled geochemical and physical transport processes governing waste-rock weathering and drainage is prone to uncertainties associated with process selection and parameterization. The consistent reactive transport model we used to simulate the widely varying waste-rock systems represents a trade-off between data availability, resolution, and quality versus model sophistication and parameter identifiability. Well-constrained processes with high-quality data allowed some processes and properties to be represented with higher confidence: we have a reasonably good control on bulk-average mineral abundances and therefore waste-rock reactivity, as well as on grain-size distributions and hydraulic (tracer tested) parameters of the waste rock. Yet, some features such as the details of internal heterogeneity within the larger-scale piles remained unquantifiable (e.g., permeability) and require calibration. The deployed 1-D single-domain approach captured trends of smaller-scale experiments with good mass balance, but it sacrificed spatiotemporal accuracy for identifiable model parameters on longer-term larger-scale experiments fit for the purpose of assessing long-term drainage patterns, but perhaps not shorter-time scale fluctuations or the geochemistry at specific internal locations. The uncertainty associated to the impact of misrepresenting internal saturation profiles on mineral rates, despite being addressed in the sensitivity analyses, remains a crucial question for the upscaling of our approach.

The presented model was applied to quantify individual processes and feedbacks contributing to drainage dynamics. Simulations show that oxygen availability reduced mineral reaction rates, predominantly in simulations of larger-scale experiments (¿10 m) with reactive (several wt-% S) waste rock. Reactive mineral surface areas estimated from physical grain size distributions provided consistent proportionality and could be used to reproduce weathering dynamics of the same rock types on different experimental scales. Finally, our reactive transport model revealed that secondary minerals play a critical role in controlling drainage quality, with key phases in the simulated experiments being based on experimental identification in prior studies (e.g., gypsum, Fe-oxyhydroxides as well as less-abundant phases such as antlerite

and brochantite). While antlerite and brochantite may serve as surrogates for all Cu-sulfates (observational data suggests low abundance and poor crystallinity), less-abundant secondary phases were crucial to reproduce certain drainage dynamics, for instance Cu mobilization under acidifying conditions in field barrel FB-I9 and experimental pile 2C. Our results highlight the use of process-oriented and field-parameterized models to resolve dynamics that are challenging to identify experimentally, especially from smaller-scale tests of shorter duration.

Overall, we have shown that a well-chosen model formulation, applied consistently and utilizing readily available parameters and thermodynamic data, can explain drainage dynamics from waste-rock systems across several orders-of magnitude different scales, while only fitting key reaction-rate parameters. Many of the most consequential properties, particularly mineral abundances, and grain size distributions, can be constrained a priori, reducing the uncertainty and number of fitting parameters that must be determined. Hence, our model formulation is useful to explain the processes in the experiments examined here and may be useful for similar and larger-scale systems. However, some processes, such as heat transport and gas migration (convection) or preferential flow (Blackmore et al., 2014), are negligible on the scales examined here. Applicability of our approach is thus restricted to relatively small-scale experiment displaying low degrees of heterogeneity. Similarly, its performance for predictive purposes remains to be demonstrated (Vriens et al., 2020), as processes affecting mineral reactivity and weathering rates on longer timescales (e.g., reduced through passivation) were not considered. Despite these uncertainties, this work demonstrates that evidence-based reactive transport models that explicitly account for key processes and are parametrized experimentally may be used to examine and possibly predict waste-rock weathering dynamics across a laboratory-to-practice scale range - contributing to improved risk management.

Acknowledgements

We would like to thank the Antamina mine staff for support during the construction, monitoring and sampling of various long-term field experiments. Financial support was provided by Compania Minera Antamina S.A., the Natural Science and Engineering Research Council of Canada (NSERC, grant CRDPJ334909-2005) and Teck Metals Limiteds Applied Research and Technology Group. The contributions by Nicolas Seigneur were supported by

the Natural Sciences and Engineering Research Council of Canada (NSERC) through the strategic network grant "Toward Environmentally Responsible Resource Extraction Network (TERRE-NET)", grant number 479708-2015. Additionally, we would like to thank Laurent Culot, for his philosophical insights in economics.

Supplementary Material

Supporting Information (Supporting Methods, Tables S1-S8 and Figures S1-S7) contains additional methodological details, parameters for the reactive transport models and additional figures related to the presented simulations.

5. References

Acker, J. and Bricker, O. (1992). The influence of ph on biotite dissolution and alteration kinetics at low temperature. Geochimica et Cosmochimica Acta, 56(8):3073–3092.

Akcil, A. and Koldas, S. (2006). Acid mine drainage (amd): causes, treatment and case studies. Journal of cleaner production, 14(12-13):1139–1145.

Amos, R. T., Blowes, D. W., Bailey, B. L., Sego, D. C., Smith, L., and Ritchie, A. I. M. (2015). Waste-rock hydrogeology and geochemistry. Applied Geochemistry, 57:140–156.

Amos, R. T., Blowes, D. W., Smith, L., and Sego, D. C. (2009). Measurement of wind-induced pressure gradients in a waste rock pile. Vadose Zone Journal, 8(4):953–962.

Appels, W. M., Ireson, A. M., and Barbour, S. L. (2018). Impact of bimodal textural heterogeneity and connectivity on flow and transport through unsaturated mine waste rock. Advances in water resources, 112:254–265.

Arora, B., Mohanty, B. P., and McGuire, J. T. (2011). Inverse estimation of parameters for multidomain flow models in soil columns with different macropore densities. Water resources research, 47(4).

Atherton, C. (2017). An investigation of heterogeneity and the impact of acidic regions on bulk effluent from a deconstructed low sulfide waste-rock pile. Master's thesis, University of Waterloo.

694 Aubertin, M., Cifuentes, E., Apithy, S., Bussière, B., Molson, J., and Cha-
695 puis, R. (2009). Analyses of water diversion along inclined covers with cap-
696 illary barrier effects. Canadian Geotechnical Journal, 46(10):1146–1164.

697 Bay, D., Peterson, H., Singurindy, O., Aranda, C., Dockrey, J., Vargas, F. S.,
698 Gallegos, J., Mayer, K., Smith, L., Klein, B., et al. (2009). Assessment of
699 neutral ph drainage from three experimental waste-rock piles at the antam-
700 ina mine, peru. In 8th International Conference on Acid Rock Drainage,
701 pages 188–199.

702 Bea, S., Wilson, S., Mayer, K., Dipple, G., Power, I., and Gamazo, P. (2012).
703 Reactive transport modeling of natural carbon sequestration in ultramafic
704 mine tailings. Vadose Zone Journal, 11(2).

705 Beckie, R., Aranda, C., Blackmore, S., Peterson, H., Hirsche, D., Javadi, M.,
706 Blaskovich, R., Haupt, C., Dockrey, J., Conlan, M., et al. (2011). A study
707 of the mineralogical, hydrological and biogeochemical controls on drainage
708 from waste rock at the antamina mine, peru: an overview. In Tailings and
709 Mine Waste 2011: Proceedings of the 15 th International Conference on
710 Tailings and Mine Waste, Vancouver, BC.

711 Beckingham, L. E., Mitnick, E. H., Steefel, C. I., Zhang, S., Voltolini, M.,
712 Swift, A. M., Yang, L., Cole, D. R., Sheets, J. M., Ajo-Franklin, J. B., et al.
713 (2016). Evaluation of mineral reactive surface area estimates for prediction
714 of reactivity of a multi-mineral sediment. Geochimica et Cosmochimica
715 Acta, 188:310–329.

716 Bethke, C. M. (2007). Geochemical and biogeochemical reaction modeling.
717 Cambridge University Press.

718 Blackmore, S., Pedretti, D., Mayer, K., Smith, L., and Beckie, R. (2018a).
719 Evaluation of single-and dual-porosity models for reproducing the release of
720 external and internal tracers from heterogeneous waste-rock piles. Journal
721 of contaminant hydrology, 214:65–74.

722 Blackmore, S., Smith, L., Mayer, K. U., and Beckie, R. D. (2014). Com-
723 parison of unsaturated flow and solute transport through waste rock at
724 two experimental scales using temporal moments and numerical modeling.
725 Journal of contaminant hydrology, 171:49–65.

726 Blackmore, S., Vriens, B., Sorensen, M., Power, I. M., Smith, L., Hallam,
727 S. J., Mayer, K. U., and Beckie, R. D. (2018b). Microbial and geochemical
728 controls on waste rock weathering and drainage quality. Science of the
729 Total Environment, 640:1004–1014.

730 Blowes, D., Ptacek, C., Jambor, J., and Weisener, C. (2003). The geochem-
731 istry of acid mine drainage. Environmental geochemistry, 9:149–204.

732 Brady, P. V. and Walther, J. V. (1989). Controls on silicate dissolution rates
733 in neutral and basic ph solutions at 25 c. Geochimica et Cosmochimica
734 acta, 53(11):2823–2830.

735 Bray, A. W., Oelkers, E. H., Bonneville, S., Wolff-Boenisch, D., Potts, N. J.,
736 Fones, G., and Benning, L. G. (2015). The effect of ph, grain size, and
737 organic ligands on biotite weathering rates. Geochimica et Cosmochimica
738 Acta, 164:127–145.

739 Brookfield, A. E., Blowes, D. W., and Mayer, K. U. (2006). Integration of field
740 measurements and reactive transport modelling to evaluate contaminant
741 transport at a sulfide mine tailings impoundment. Journal of contaminant
742 hydrology, 88(1-2):1–22.

743 Carrera, J. and Neuman, S. P. (1986). Estimation of aquifer parameters
744 under transient and steady state conditions: 2. uniqueness, stability, and
745 solution algorithms. Water Resources Research, 22(2):211–227.

746 Chou, L. and Wollast, R. (1985). Steady-state kinetics and dissolution mech-
747 anisms of albite. American Journal of Science, 285(10):963–993.

748 Conlan, M., Mayer, K. U., Blaskovich, R., and Beckie, R. D. (2012). Sol-
749 ubility controls for molybdenum in neutral rock drainage. Geochemistry:
750 Exploration, Environment, Analysis, 12(1):21–32.

751 Demers, I., Molson, J., Bussière, B., and Laflamme, D. (2013). Numerical
752 modeling of contaminated neutral drainage from a waste-rock field test
753 cell. Applied geochemistry, 33:346–356.

754 Dove, P. (1995). Geochemical controls on the kinetics of quartz fracture at
755 subcritical tensile stresses. Journal of Geophysical Research: Solid Earth,
756 100(B11):22349–22359.

Elghali, A., Benzaazoua, M., Bussière, B., and Bouzahzah, H. (2019). Determination of the available acid-generating potential of waste rock, part ii: Waste management involvement. Applied geochemistry, 100:316–325.

Erguler, Z. A. and Erguler, G. K. (2015). The effect of particle size on acid mine drainage generation: Kinetic column tests. Minerals Engineering, 76:154–167.

Harrison, B., Aranda, C., Sanchez, M., and Vizconde, J. (2012). Waste rock management at the antamina mine: Overall management and data application in the face of continued expansion. In Proceedings of the 9th International Conference on Acid Rock Drainage (ICARD), Ottawa, ON, Canada, pages 1176–1187.

Haug, M. and Pauls, G. (2002). A review of non-traditional dry covers. Canada: MEND Report 2.21.3b - available online.

Hirsche, D. T., Blaskovich, R., Mayer, K. U., and Beckie, R. D. (2017). A study of zn and mo attenuation by waste-rock mixing in neutral mine drainage using mixed-material field barrels and humidity cells. Applied Geochemistry, 84:114–125.

Hudson-Edwards, K. and Dold, B. (2015). Mine waste characterization, management and remediation. Minerals, 5:82–85.

Jeen, S.-W., Mayer, K. U., Gillham, R. W., and Blowes, D. W. (2007). Reactive transport modeling of trichloroethene treatment with declining reactivity of iron. Environmental science & technology, 41(4):1432–1438.

Kimball, B., Rimstidt, J., and Brantley, S. (2010). Chalcopyrite dissolution rate laws. Applied Geochemistry, 25.7:972–983.

Lahmira, B., Lefebvre, R., Aubertin, M., and Bussière, B. (2017). Effect of material variability and compacted layers on transfer processes in heterogeneous waste rock piles. Journal of contaminant hydrology, 204:66–78.

Langman, J. B., Moore, M. L., Ptacek, C. J., Smith, L., Sego, D., and Blowes, D. W. (2014). Diavik waste rock project: Evolution of mineral weathering, element release, and acid generation and neutralization during a five-year humidity cell experiment. Minerals, 4(2):257–278.

Lasaga, A. C. and Kirkpatrick, J. (2018). Kinetics of geochemical processes, volume 8. Walter de Gruyter GmbH & Co KG.

Lawrence, R. and Wang, Y. (1996). Determination of neutralization potential for acid rock drainage prediction. MEND project, 1(3):38.

Lefebvre, R., Hockley, D., Smolensky, J., and Gélinas, P. (2001). Multiphase transfer processes in waste rock piles producing acid mine drainage: 1: Conceptual model and system characterization. Journal of Contaminant Hydrology, 52(1-4):137–164.

Levenspiel, O. (1998). Chemical reaction engineering book, 3rd edn, chap. 9 and 10.

Lindsay, M. B., Blowes, D. W., Condon, P. D., and Ptacek, C. J. (2009). Managing pore-water quality in mine tailings by inducing microbial sulfate reduction. Environmental science & technology, 43(18):7086–7091.

Linklater, C. M., Sinclair, D. J., and Brown, P. L. (2005). Coupled chemistry and transport modelling of sulphidic waste rock dumps at the aitik mine site, sweden. Applied Geochemistry, 20(2):275–293.

Love, D. A., Clark, A. H., and Glover, J. K. (2004). The lithologic, stratigraphic, and structural setting of the giant antamina copper-zinc skarn deposit, ancash, peru. Economic Geology, 99(5):887–916.

Maest, A. S. and Nordstrom, D. K. (2017). A geochemical examination of humidity cell tests. Applied Geochemistry, 81:109–131.

Malmström, M. E., Destouni, G., Banwart, S. A., and Strömberg, B. H. (2000). Resolving the scale-dependence of mineral weathering rates. Environmental science & technology, 34(7):1375–1378.

Martin, V., Bussière, B., Plante, B., Pabst, T., Aubertin, M., Medina, F., Bréard-Lanoix, M., Dimech, A., Dubuc, J., Poaty, B., et al. (2017). Controlling water infiltration in waste rock piles: Design, construction, and monitoring of a large-scale in-situ pilot test pile. In Proceedings of the 70th Canadian Geotechnical Society Conference, volume 70.

Mayer, K., Benner, S., Blowes, D., and Frind, E. (1999). The reactive transport model min3p: application to acid mine drainage generation and

819 treatment-nickel rim mine site, sudbury, ontario. Mining and Environment,
820 1:145–154.

821 Mayer, K. U., Frind, E. O., and Blowes, D. W. (2002). Multicomponent re-
822 active transport modeling in variably saturated porous media using a gen-
823 eralized formulation for kinetically controlled reactions. Water Resources
824 Research, 38(9):13–1.

825 Mayer, K. U. and MacQuarrie, K. T. (2010). Solution of the momas reactive
826 transport benchmark with min3pmodel formulation and simulation results.
827 Computational Geosciences, 14(3):405–419.

828 Molson, J., Aubertin, M., and Bussière, B. (2012). Reactive transport mod-
829 elling of acid mine drainage within discretely fractured porous media:
830 Plume evolution from a surface source zone. Environmental modelling
831 & software, 38:259–270.

832 Moreira, P. H., Van Genuchten, M. T., Orlande, H. R., and Cotta, R. M.
833 (2016). Bayesian estimation of the hydraulic and solute transport prop-
834 erties of a small-scale unsaturated soil column. Journal of Hydrology and
835 Hydromechanics, 64(1):30–44.

836 Nickel, E. (1973). Experimental dissolution of light and heavy minerals in
837 comparison with weathering and intrastratal solution. Contributions to
838 Sedimentology, 1:1–68.

839 Pabst, T., Molson, J., Aubertin, M., and Bussière, B. (2017). Reactive
840 transport modelling of the hydro-geochemical behaviour of partially ox-
841 idized acid-generating mine tailings with a monolayer cover. Applied
842 geochemistry, 78:219–233.

843 Pan, Z., Ye, L., Liu, T., Cheng, Z., Gao, W., and Yang, Y. (2012). A
844 simulation experimental study on oxidative kinetics of sphalerite under
845 hypergene condition. Chinese Journal of Geochemistry, 31(4):457–464.

846 Pedretti, D., Mayer, K. U., and Beckie, R. D. (2017). Stochastic multi-
847 component reactive transport analysis of low quality drainage release from
848 waste rock piles: Controls of the spatial distribution of acid generating and
849 neutralizing minerals. Journal of contaminant hydrology, 201:30–38.

Plante, B., Bussière, B., and Benzaazoua, M. (2014). Lab to field scale effects on contaminated neutral drainage prediction from the tio mine waste rocks. Journal of Geochemical Exploration, 137:37–47.

Price, W. A. (2009). Prediction manual for drainage chemistry from sulphidic geologic materials. CANMET Mining and Mineral Sciences Laboratories, Canada.

Raymond, K., Seigneur, N., Su, D., and Mayer, K. (2020a). Parameter influence on the evolution of effluent quality within numerical models of waste rock piles. Mine Water and the environment. In review.

Raymond, K., Seigneur, N., Su, D., Plante, B., Poaty, B., Bussiere, B., and Mayer, K. (2020b). Numerical modeling of a laboratory-scale waste rock pile featuring an engineered cover system. Minerals. In Review.

Rimstidt, J., Chermak, J., and Gagen, P. (1994). Rates of reaction of galena, sphalerite, chalcopyrite, and arsenopyrite with Fe (III) in acidic solutions. ACS Publications.

Ritchie, A. (1994). Sulfide oxidation mechanisms: controls and rates of oxygen transport. The environmental geochemistry of sulfide mine wastes, pages 201–245.

Salazar, P., Cama, J., Ayora, C., and Andrés, M. (2009). Chalcopyrite dissolution rate law from ph 1 to 3. Geologica Acta, 7(3):389–397.

Sapsford, D. J., Bowell, R., Dey, M., and Williams, K. P. (2009). Humidity cell tests for the prediction of acid rock drainage. Minerals Engineering, 22(1):25–36.

Seigneur, N., Mayer, K. U., and Steefel, C. I. (2019). Reactive transport in evolving porous media. Reviews in Mineralogy and Geochemistry, 85(1):197–238.

Sherlock, E., Lawrence, R., and Poulin, R. (1995). On the neutralization of acid rock drainage by carbonate and silicate minerals. Environmental Geology, 25(1):43–54.

Shokri, B. J., Ardejani, F. D., Ramazi, H., and Moradzadeh, A. (2016). Predicting pyrite oxidation and multi-component reactive transport processes

881 from an abandoned coal waste pile by comparing 2d numerical modeling
882 and 3d geo-electrical inversion. International Journal of Coal Geology,
883 164:13–24.

884 Singer, P. C. and Stumm, W. (1970). Acidic mine drainage: the rate-
885 determining step. Science, 167(3921):1121–1123.

886 Skierszkan, E., Mayer, K., Weis, D., and Beckie, R. (2016). Molybdenum and
887 zinc stable isotope variation in mining waste rock drainage and waste rock
888 at the antamina mine, peru. Science of the Total Environment, 550:103–
889 113.

890 St-Arnault, M., Vriens, B., Blaskovich, R., Aranda, C., Klein, B., Mayer,
891 K. U., and Beckie, R. D. (2020). Geochemical and mineralogical assess-
892 ment of reactivity in a full-scale heterogeneous waste-rock pile. Minerals
893 Engineering, 145:106089.

894 St.Arnault, M., Vriens, B., Klein, B., Mayer, K. U., and Beckie, R. D. (2019).
895 Mineralogical controls on drainage quality during the weathering of waste
896 rock. Applied Geochemistry, 108.

897 Stockwell, J., Smith, L., Jambor, J. L., and Beckie, R. (2006). The rela-
898 tionship between fluid flow and mineral weathering in heterogeneous un-
899 saturated porous media: A physical and geochemical characterization of a
900 waste-rock pile. Applied geochemistry, 21(8):1347–1361.

901 Strömberg, B. and Banwart, S. (1999). Weathering kinetics of waste rock
902 from the aitik copper mine, sweden: scale dependent rate factors and ph
903 controls in large column experiments. Journal of Contaminant Hydrology,
904 39(1-2):59–89.

905 Su, D., Mayer, K. U., and MacQuarrie, K. T. (2017). Parallelization of
906 min3p-thcm: A high performance computational framework for subsur-
907 face flow and reactive transport simulation. Environmental Modelling &
908 Software, 95:271–289.

909 Trinchero, P., Beckie, R., Sanchez-Vila, X., and Nichol, C. (2011). Assessing
910 preferential flow through an unsaturated waste rock pile using spectral
911 analysis. Water Resources Research, 47(7).

Vriens, B., Arnault, M. S., Laurenzi, L., Smith, L., Mayer, K. U., and Beckie, R. D. (2018). Localized sulfide oxidation limited by oxygen supply in a full-scale waste-rock pile. Vadose Zone Journal, 17(1).

Vriens, B., Peterson, H., Laurenzi, L., Smith, L., Aranda, C., Mayer, K. U., and Beckie, R. D. (2019a). Long-term monitoring of waste-rock weathering at the antamina mine, peru. Chemosphere, 215:858–869.

Vriens, B., Seigneur, N., Mayer, K. U., and Beckie, R. D. (2020). Scale dependence of effective geochemical rates in weathering mine waste rock. Journal of Contaminant Hydrology, 234:103699.

Vriens, B., Skierszkan, E. K., St-Arnault, M., Salzsauler, K., Aranda, C., Mayer, K. U., and Beckie, R. D. (2019b). Mobilization of metal (oid) oxyanions through circumneutral mine waste-rock drainage. ACS omega, 4(6):10205–10215.

Vriens, B., Smith, L., Mayer, K. U., and Beckie, R. D. (2019c). Poregas distributions in waste-rock piles affected by climate seasonality and physicochemical heterogeneity. Applied geochemistry, 100:305–315.

Williamson, M. A. and Rimstidt, J. D. (1994). The kinetics and electrochemical rate-determining step of aqueous pyrite oxidation. Geochimica et Cosmochimica Acta, 58(24):5443–5454.

Wilson, D., Amos, R. T., Blowes, D. W., Langman, J. B., Ptacek, C. J., Smith, L., and Sego, D. C. (2018). Diavik waste rock project: A conceptual model for temperature and sulfide-content dependent geochemical evolution of waste rock–laboratory scale. Applied geochemistry, 89:160–172.

Wösten, J. H. M. and Van Genuchten, M. T. (1988). Using texture and other soil properties to predict the unsaturated soil hydraulic functions. Soil Science Society of America Journal, 52(6):1762–1770.

Wunderly, M., Blowes, D., Frind, E., and Ptacek, C. (1996). Sulfide mineral oxidation and subsequent reactive transport of oxidation products in mine tailings impoundments: A numerical model. Water Resources Research, 32(10):3173–3187.